J. Fluid Mech. (1967), *vol.* 27, *part* 2, *pp.* 231–252
Printed in Great Britain

Jet diffusion in the region of flow establishment

By SEDAT SAMI, THOMAS CARMODY AND HUNTER ROUSE
Institute of Hydraulic Research, The University of Iowa, Iowa City

(Received 21 March 1966)

In the flow-establishment region of an air jet issuing with an efflux velocity of about 35 ft./sec from a 1·0 ft. diameter nozzle into still air, measurements were made of mean axial and radial velocities, mean static pressure, turbulence intensities, turbulent shear, and pressure fluctuation. For the measurement of the latter a pressure probe using a ceramic piezo-electric tube was developed. Also included in the measurements were the temporal mean gradient and auto-correlation of the axial-velocity fluctuation and the intermittency factor. The fluctuating-pressure and turbulence-intensity fields were observed to be closely similar in form. Through use of the measured distributions of mean-flow and turbulence characteristics, all terms of the integral and differential forms of the momentum and mean-energy equations were evaluated throughout the region. The results are presented herein by curves of variation of each of the terms as they appear in the corresponding equations.

1. Introduction

A previous investigation described by one of the authors (Rouse 1953) involved an attempt to correlate the phenomenon of jet diffusion with that of cavitation, to the end of predicting conditions under which vaporization would begin to occur at the cores of the turbulent eddies. Experimental data were readily obtained for various stages of jet cavitation, and provisional measurements were also made of pressure fluctuations in the jet without cavitation. Continued study of the cavitating jet, however, only emphasized the statistical nature of the occurrence, and further efforts to measure fluctuating pressures met more often with failure than with success. Even the seemingly routine measurement of velocity fluctuations began to disclose difficulties, in zones of intermittency as well as zones of high relative intensity.

As a result of these troublesome matters, a threefold attack upon the general problem has been under way at the Iowa Institute for the past decade. The cavitation aspect, dependent as it is upon the other two, is progressing more slowly and will have no further part in the present paper. The turbulence aspect has been looked into experimentally under a number of different boundary situations: the hydraulic jump (Rouse, Siao & Nagaratnam 1959), abrupt conduit expansions (Chaturvedi 1963), the wake of a disk (Carmody 1964), and the wakes of self-propelled bodies (Naudascher 1965); not only were the primary characteristics of the mean and turbulent flows measured in detail, but the measure-

ments were found to satisfy the requirements of the integrated momentum and energy equations with successively better approximation. Finally, attention has been given as well to the reproducible measurement of the fluctuating pressure. Though the technique of pressure–velocity correlation is still under development, all the terms of the mean-energy equation for the diffusing jet are now at hand in reasonably precise form, and it is these (together with the pressure fluctuations) which are of interest in the further analysis of jet cavitation. The measurements and their satisfaction of the differential and integral forms of the momentum and mean-energy equations are presented herein.

2. Experimental equipment and techniques

2.1. *Test facilities*

In order to determine the flow characteristics in the vicinity of the efflux section with sufficient detail, a nozzle diameter of 1·0 ft. was selected for the principal experiments. The task of providing a correspondingly large duct was avoided by

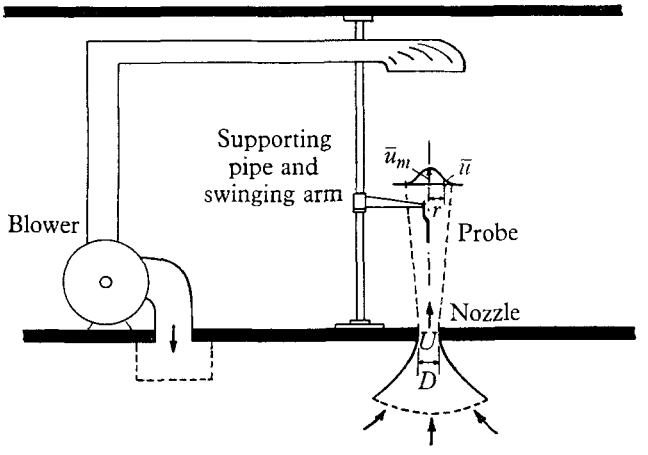

FIGURE 1. Schematic diagram of test set-up.

using a $30 \times 15 \times 12$ ft. room as a test chamber, setting the carefully turned and varnished nozzle vertically in the floor, providing a screened conical approach in the ceiling of the room below, and exhausting the air from the test room by means of a $1\frac{1}{2}$ horsepower blower, as shown schematically in figure 1. (To ensure axial symmetry, an extension of the blower intake was located directly over the nozzle.) For measurements 6 or more diameters from the efflux section, a 0·5 ft. nozzle insert could be utilized, and conditions relatively far out in the diffusing jet were checked above a 0·2 ft. nozzle in apparatus used in student instruction. A very few measurements were conducted just beyond the $3\frac{1}{2}$ ft. nozzle of an open-throat air tunnel. The experiments with the 1 ft. nozzle were carried out at an efflux velocity U of about 35 ft./sec, corresponding to an exit Reynolds number of 22×10^4.

As an instrument carriage a selected length of 3 in. pipe was mounted vertically between floor and ceiling beams 3 ft. from the jet axis, and a rotating arm that

could be hinged therefrom at any elevation swung in an arc over the jet cross-section. The instrument mounted on the arm could thus be placed at any desired radial and longitudinal position with respect to the efflux section.

2.2. *Measuring equipment*

Four types of probe were used: a static tube, for mean ambient pressure; a single-wire anemometer probe, for the axial components of the mean velocity and of the fluctuation, the auto-correlation, the dissipation length, and the intermittency factor; a cross-wire anemometer probe, for both the axial and radial components of the mean velocity, the three (axial, radial, and tangential) components of the fluctuation, and the turbulent shear; and a piezo-electric ceramic probe, shown in figure 2, for the pressure fluctuation.

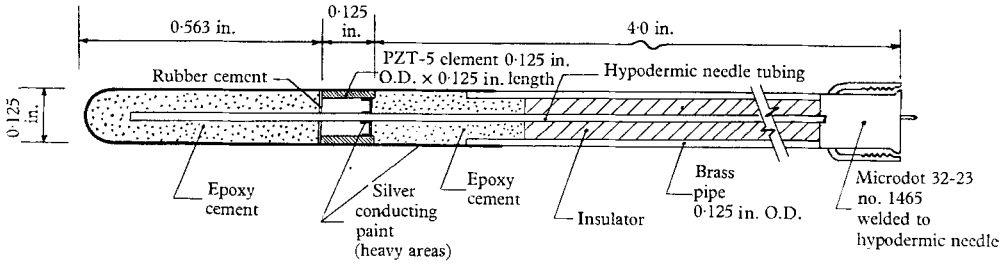

FIGURE 2. Probe used to measure pressure fluctuation.

The ambient-pressure probe was made from a 0·049 in. diameter hypodermic needle with a solid rounded nose. Four equally spaced 0·010 in. diameter holes were drilled radially into the probe at a distance of 10 tube diameters from the tip. The differential pressure obtained from the tube was read to 0·001 in. of alcohol on a micromanometer having a range of 0–3 in.

The sensing elements of the anemometer probes were made of 0·00012 in. diameter tungsten wire having 10 % platinum coating. The wire was copper plated and etched to a cold resistance of about 5 ohms.

The basic anemometer circuit was of the linearized constant-temperature type, used in conjunction with a mean-square analyser and a digital voltmeter, all of Iowa Institute manufacture. For the auto-correlation and differentiation measurements, use was made of an Old Gold Model 4-2 anemometer and an Old Gold Model D Type 2 mean-product computer manufactured by the Hubbard Instrument Company. The latter instrument made possible the measurement of mean-velocity components (axial and radial) by the use of the cross-wire probe and hence provided an effective way of checking the data collected through the use of the single-wire probe. A Type 802 G 1 delay line manufactured by AD-YU Electronics Laboratory, Inc., and an Iowa Institute delay-line driver were used during auto-correlation measurements. Mean-velocity hot-wire calibrations were carried out at the beginning and the end of each series of runs: A stagnation tube connected to a micromanometer was placed in the 'potential' cone at the efflux section. Next, the efflux velocity was varied over a wide range by controlling the intake to the blower while stagnation-pressure and hot-wire-anemometer

readings were recorded simultaneously. In zones of high-intensity turbulence—i.e. wherever the visual signal was strongly fluctuating—accuracy in obtaining the mean value of the random signal was considerably increased by reading the display of an electronic counter into which the signal was fed. For the analysis of intermittency, an analyser employing an entirely new approach to the problem has been designed at the Iowa Institute (Glover 1965). Three additional instruments are needed for its operation. The first is the Old Gold Model anemometer already described. It is used not only to obtain the hot-wire signal, but also to supply the power necessary to operate the Intermittency Analyzer. The second instrument is an electronic counter (Computer Measurements Company Model 603A) with a 10,000 c/s continuous output which is fed back into and gated by the intermittency circuit to give the intermittency factor. The third instrument is an oscilloscope such as the one manufactured by Hewlett-Packard, Model 120B.

The pressure probe contained a piezo-electric ceramic tube of the radially polarized thickness-expander type (model PZT-5) manufactured by the Clevite Corporation. The amplification circuit used in connexion with it contained a low-noise high-impedance pre-amplifier (Model 143 manufactured by Ithaco, Inc.) with a gain of 40 dB. The probe was calibrated by placing it in a lucite-walled chamber and comparing its signal to that of a calibrated Altec-Lansing 21BR180 microphone. Because of the frequency range over which the probe was calibrated (25 to 800 c/s) no attempt was made to eliminate reflexion of the sound waves within the chamber. The source used for the signals was a Ling–Altec Model ID-60 driver powered by a Heathkit sine-square generator Model IG-B2 through a Ling–Altec amplifier. The main emphasis in the design and manufacture of the probes was on obtaining the smallest possible diameter, a sufficiently high signal-to-noise ratio, and a resonant frequency beyond the frequency range of the present study. The piezo-electric ceramic tubes tested were of various diameters (0·250, 0·125 and 0·063 in.), their sensitivity depending mainly on the radius-to-wall thickness ratio. The equation of resonant frequencies did not pose any serious problem, but the first two opposing requirements led to a compromise between the size of the probe and its sensitivity. Eventually, for the region of flow establishment, a signal-to-noise ratio of about 7 was achieved with tubes 0·125 in. in diameter.

3. Evaluation and discussion of results

Hot-wire and pressure-probe traverses were carried out at sections with x/D ratios of 1, 2, 3, 4, 5, 6, 8, 10, 12, and 20. At each section, radial traverses covered the entire field of turbulent flow. The results of measurements for sections with x/D ratios of 1, 3, 6, and 10, all within the region of flow establishment, are given herein, after being rendered dimensionless. Computed values at points symmetrical with respect to the jet axis were first averaged and the results presented for the half-jet only. As for the region of established flow, it may suffice to add that the data at hand for the mean- and fluctuating-velocity fields compare satisfactorily with those published elsewhere (Dai 1947; Corrsin 1947; Baines 1948; Corrsin & Uberoi 1949; Hinze & Van der Hegge Zijnen 1949; Alexander, Baron & Comings 1953).

3.1. *Mean-flow characteristics*

The axial component of the mean velocity was initially determined using a single-wire probe. Later on, the Old Gold Model 4-2 anemometer became available, and hence check readings using a cross-wire probe were made possible. Except at the outer edge of the mixing region, the two sets of results were in good agreement. Figure 3 shows the distribution of relative mean axial velocity $\bar{u}/U$ throughout the field of measurement.

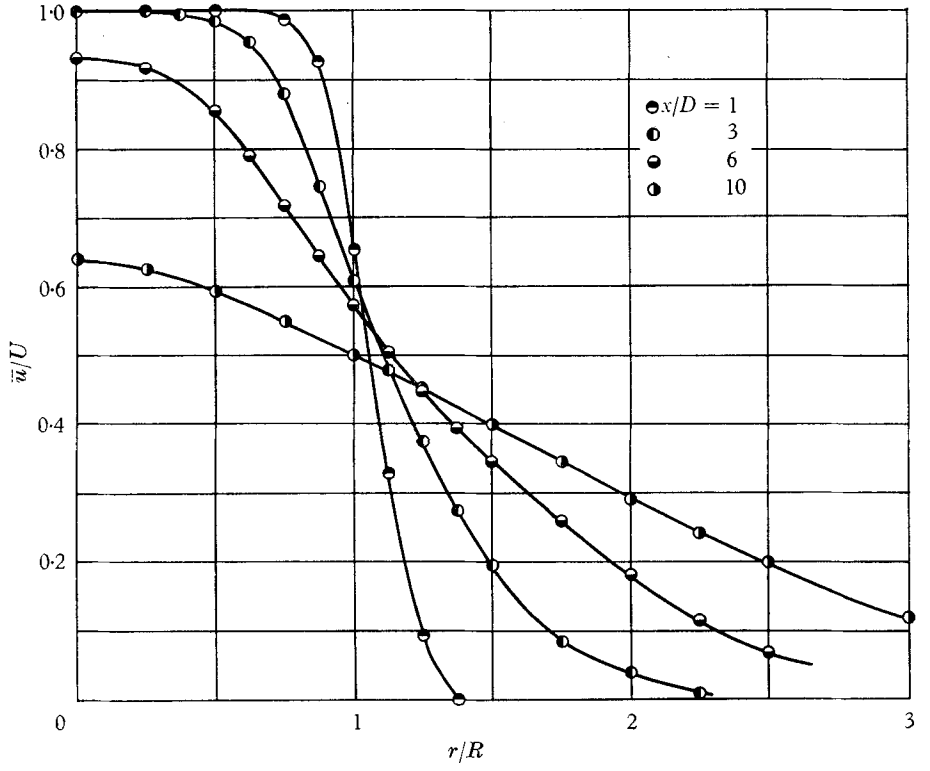

FIGURE 3. Mean axial-velocity profiles.

The mean radial component $\bar{v}$ was first determined through the continuity relationship, using for $\bar{u}$ the values obtained from single-wire measurements. However, as in the case of the axial component, use was later made of the new anemometer circuitry to measure $\bar{v}$ with a cross-wire probe. Figure 4 shows the measured distribution of relative mean radial velocity $\bar{v}/U$, together with the values computed from continuity requirements. The discrepancies can best be explained by the fact that in the outer edge of the mixing region the axial component of the velocity is no longer large compared with the radial; therefore, the indication of the single wire can no longer be assumed equal to the axial component of the velocity.

Since the mean ambient pressures throughout the field of measurement were obtained with a tube upon which the effect of turbulence was assumed negligible,

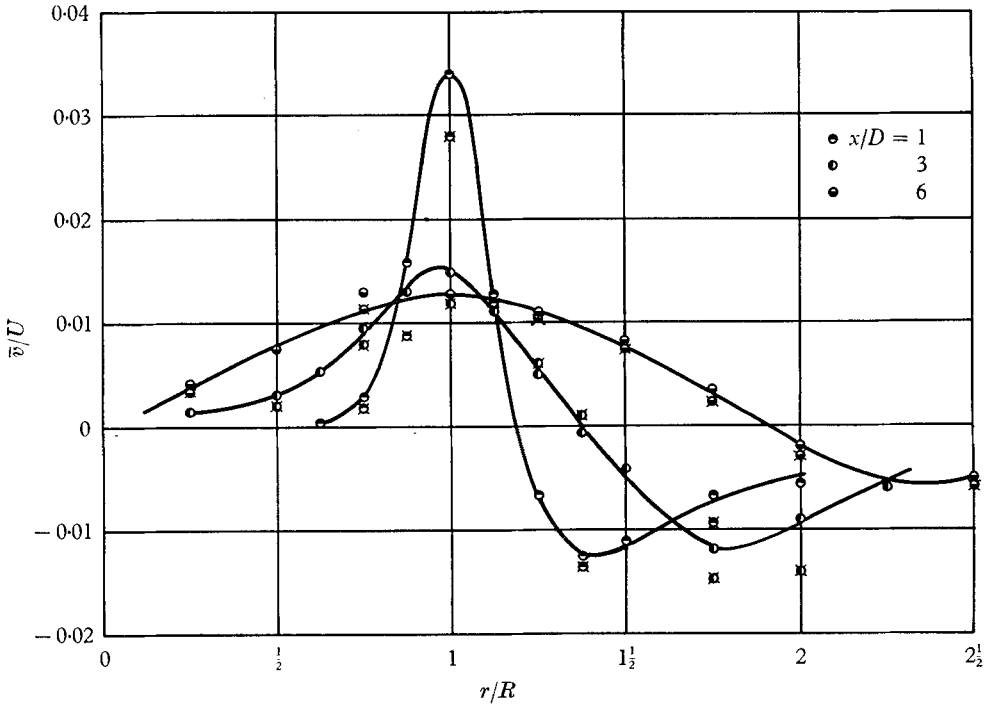

FIGURE 4. Mean radial-velocity profiles. Computed values are shown by crosses.

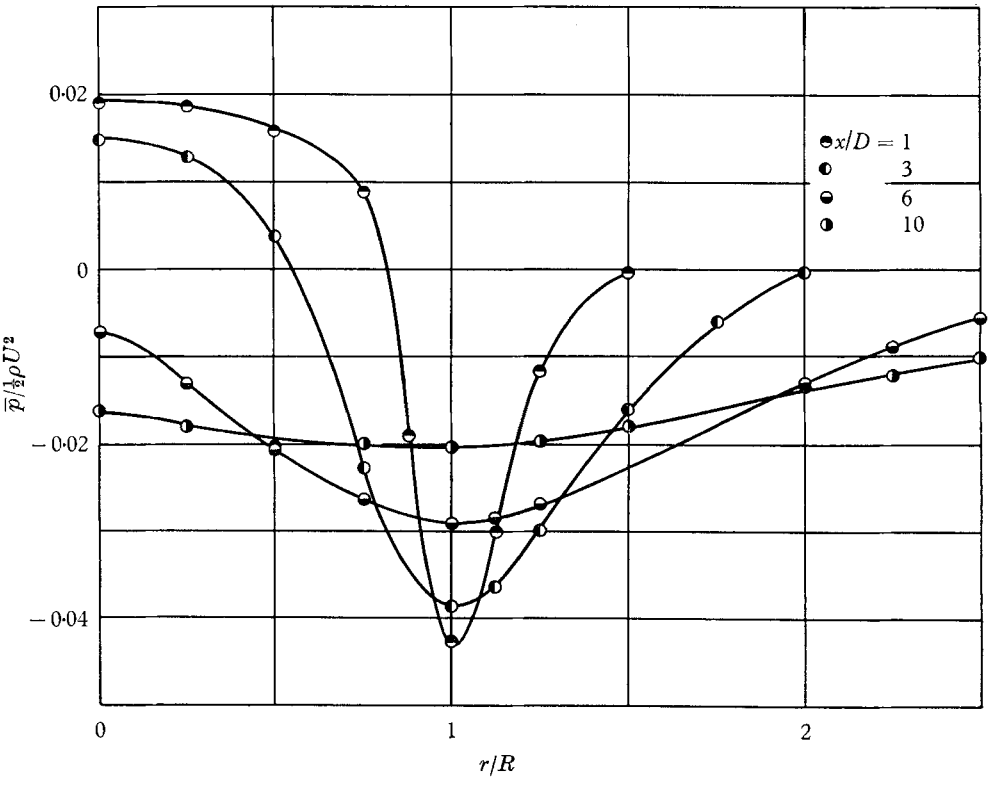

FIGURE 5. Mean ambient-pressure profiles.

no correction was applied to the indicated pressure measurements. Figure 5 represents a non-dimensional plot of $\overline{p}/\frac{1}{2}\rho U^2$ *vs.* radial position. It confirms several striking features of an earlier two-dimensional jet study (Miller & Comings 1957). The persistence of the positive ambient pressure within the potential cone for a few diameters downstream from the efflux section, and the presence of negative pressure everywhere outside of the cone, should be noted.

3.2. *Turbulence characteristics*

Mean-square axial turbulence intensities were measured throughout the region with the help of the single-wire probe. At three sections downstream from the nozzle, the radial and tangential components of the fluctuation were also obtained

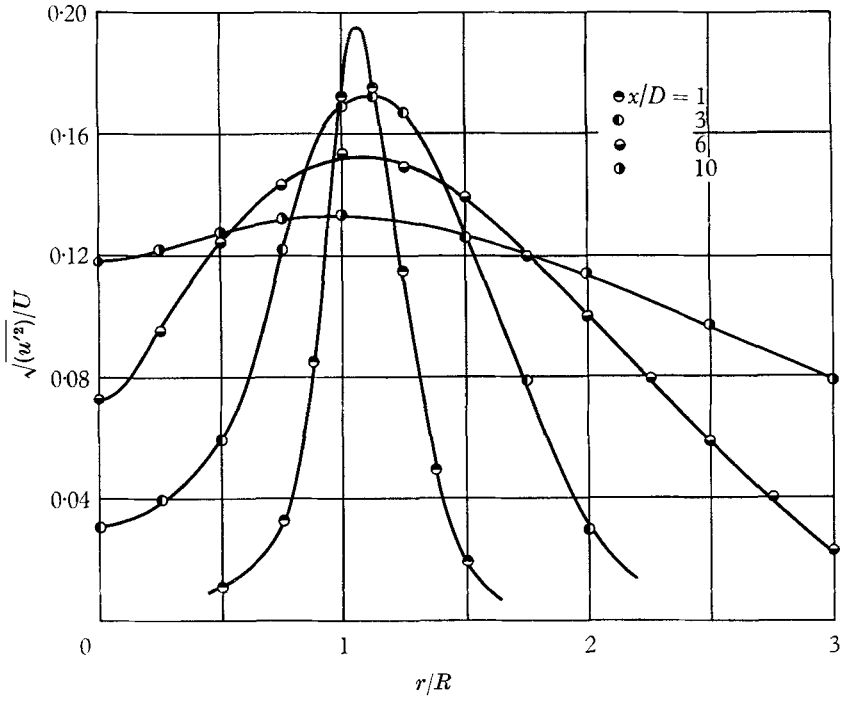

FIGURE 6. Axial velocity-fluctuation profiles.

using a cross-wire probe. A comparative analysis of the results gave strong support for the use of $\overline{u'^2} \simeq 2\overline{v'^2}$ and $\overline{u'^2} \simeq 2\overline{w'^2}$ as close approximations in evaluating some of the terms of the axial-momentum and mean-energy equations. Figures 6 and 7 show the distributions of the relative root-mean-square axial turbulence intensity $\sqrt{(\overline{u'^2})}/U$ and the mean turbulent shear $\overline{u'v'}/U^2$ in the field of flow.

In figure 8 the relative values of the root-mean-square pressure fluctuation $\sqrt{(\overline{p'^2})}/\frac{1}{2}\rho U^2$ are plotted *vs.* r/R. Obviously, the relative size of the pressure probe with respect to the scale of an 'average' eddy is too large in the vicinity of the nozzle. Auto-correlation measurements conducted throughout the mixing zone indicate that, immediately downstream from the efflux section, such an eddy scale is indeed of the same order of magnitude as the diameter of the probe. That

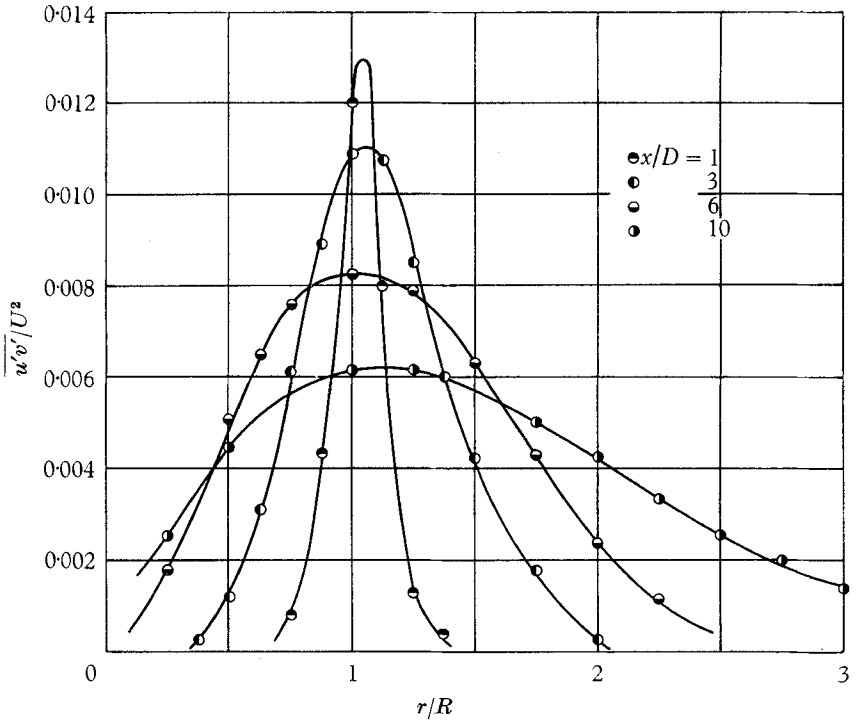

FIGURE 7. Turbulent-shear profiles.

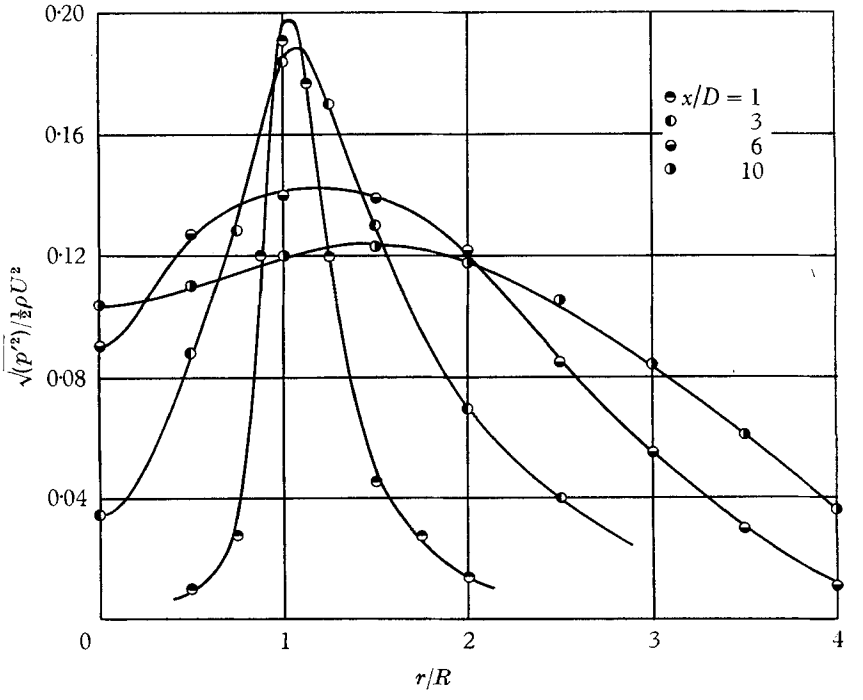

FIGURE 8. Pressure-fluctuation profiles.

the data for this region would be somewhat less accurate than those at sections farther downstream was, therefore, to be expected. Evidence of this situation was obtained by using the $3\frac{1}{2}$ ft. nozzle of the open-throat air tunnel; then the probe, placed at the same dimensionless distance x/D as before, indicated appreci-

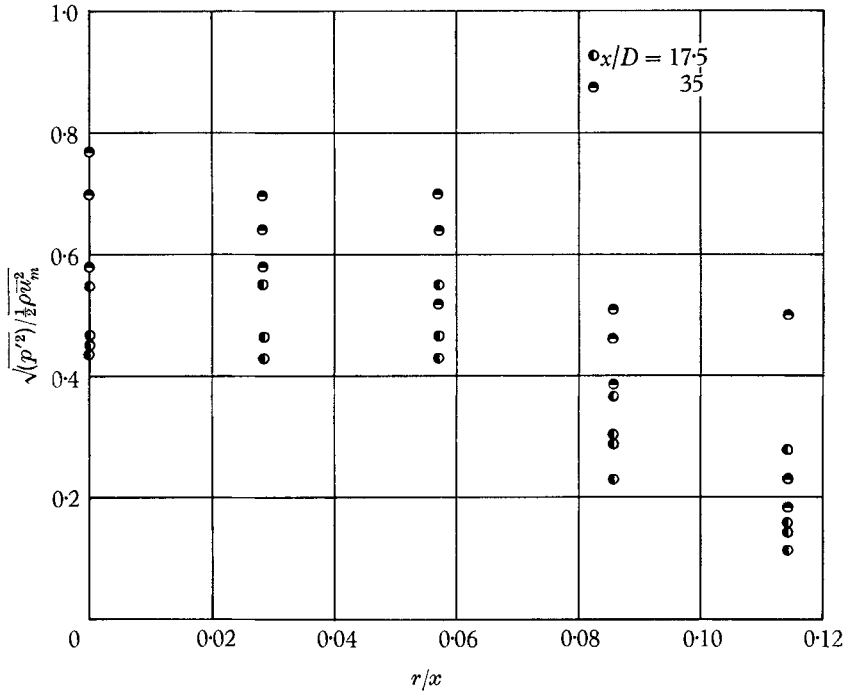

FIGURE 9. Pressure fluctuation in the region of established flow.

ably increased signals when compared with the data of the 1 ft. nozzle. In figure 9 three arbitrary sets of runs at two downstream sections are presented in the form of a plot of the relative pressure fluctuation $\sqrt{(\overline{p'^2})}/\frac{1}{2}\rho\overline{u}_m^2$ *vs.* r/x. The experiments were carried out with two nozzles, 0·1 and 0·2 ft. in diameter. The signal-to-noise ratio of the pressure probe, and hence its sensitivity, decreases near the outer edge of the jet and within the zone of established flow. Increased efflux velocity, on the other hand, resulted in the generation of some additional noise. The scatter of the data in figure 9 can therefore be explained best by the reduced sensitivity of the pressure probe in zones of low turbulence intensity.

The effect of fluctuating cross-velocities upon the indications of the pressure probe has been analysed by Strasberg (1963) and the mean-square error involved in the measured pressure compared with the magnitude of the pressure fluctuation itself. He concluded that, although in isotropic turbulence the estimated magnitude of the static-pressure fluctuation is of the same order of magnitude as the error and therefore impossible to measure, the pressure fluctuation in the wake behind a cylinder was some four times as large as the error due to the fluctuating cross-velocities. In a similar study of the pressure fluctuation behind a cylinder, Kobashi (1957) has also obtained results indicating that the dynamic

pressures due to cross-velocities and contributing to the fluctuating static-pressure signal were negligible. During the present study no correction was introduced into the indicated measurement of fluctuating static pressure. A comparison between the spatial distribution of the intensity of fluctuating pressure and that of the intensity of axial turbulence suggests a somewhat constant relationship between the two. It is interesting to note that Strasberg's measurements in the wake of a cylinder and at the section $x/D = 24$ yield for the ratio $\sqrt{(\overline{p'^2})}/\frac{1}{2}\rho\overline{u'^2}$ a value of about 2·9 compared with 1·16 for the isotropic case.

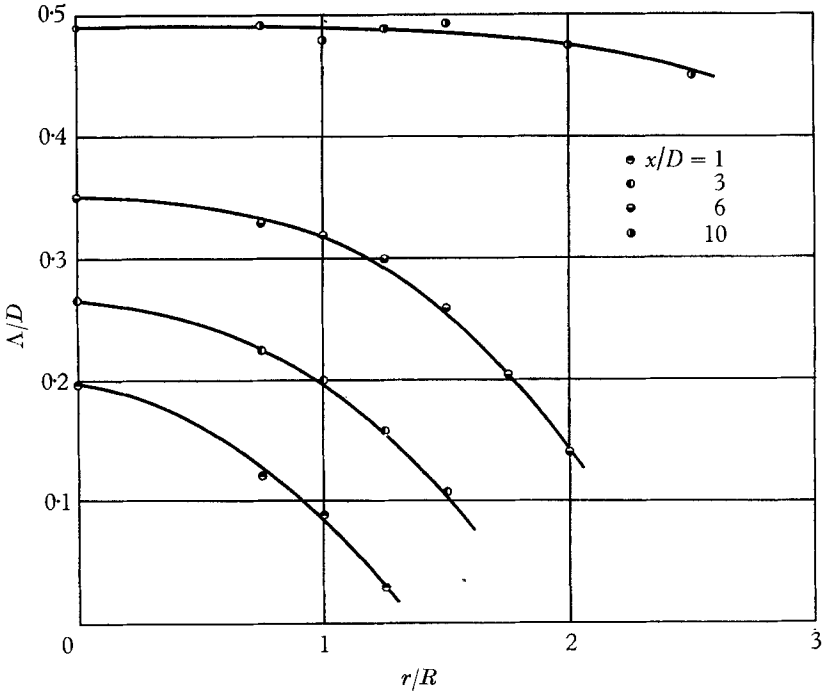

FIGURE 10. Average eddy scale.

On the other hand, the results of the jet studies presently discussed indicate for the region of flow establishment a ratio of about 6. Although near the outer edge of the jet the reduced sensitivity of the pressure probe seems to result in somewhat larger ratios, throughout the rest of the region of flow establishment the ratio $\sqrt{(\overline{p'^2})}/\frac{1}{2}\rho\overline{u'^2}$ remains fairly constant.

3.3. *Average eddy and dissipation scales*

The area under the auto-correlation curve multiplied by the local mean axial velocity yields a characteristic length Λ defined as the 'average eddy scale'. The auto-correlation coefficient is defined as

$$R_t = [\overline{u'(t).u'(t+\delta t)}]/\overline{u'(t)^2},$$

where δt represents the delay time. The 'average eddy scale' is in turn defined by $\Lambda = \overline{u}\int R_t d(\delta t)$. A non-dimensional distribution of Λ/D across the turbulent-flow field is given in figure 10. Of interest was a comparison of the auto-correlation

data with those presented by Laurence (1956). The average eddy scale resulting from the latter, after being rendered dimensionless, indicated good agreement with the former. That the mean eddy scale depends almost wholly upon the geometry of the mean flow itself was thus confirmed, since the two sets of experiments were carried out at different efflux velocities. In a previous study (Davies, Fisher & Barratt 1963), Laurence's results for the longitudinal scale of turbulence were also compared and good agreement observed.

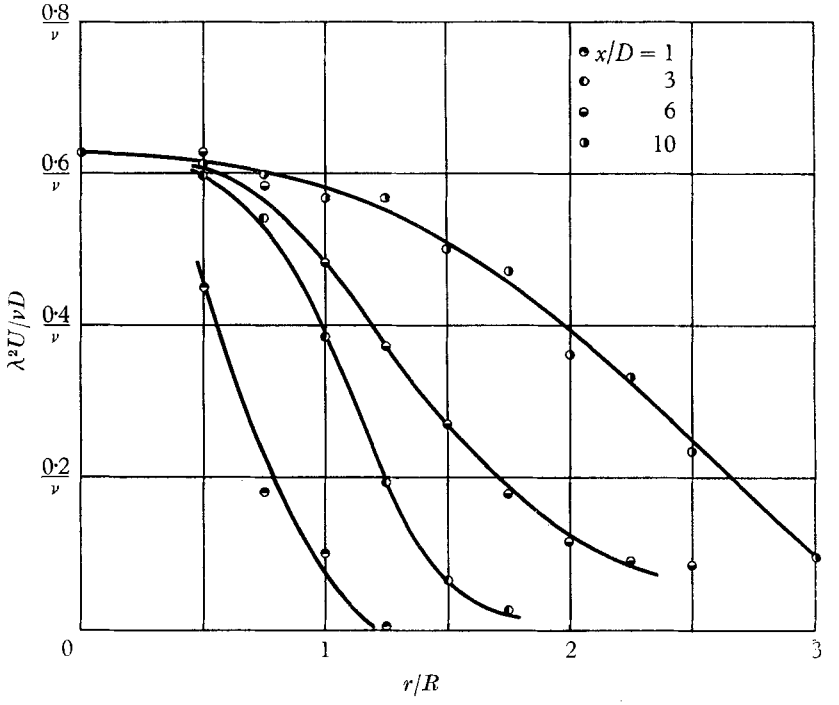

FIGURE 11. Dissipation length.

Further insight into the eddy structure of the turbulence was obtained through the study of its microscale, the 'dissipation length' λ, which is defined as $\lambda^2 = \overline{u'^2}/\overline{(\partial u'/\partial x)^2}$. On the basis of the usual assumptions of isotropic turbulence and of the undisturbed transport of turbulence characteristics—and hence of eddies—over the field, the dissipation length was computed from the measured mean-square temporal gradient of the axial-velocity fluctuation. Figure 11 shows the distribution of the dissipation length, in non-dimensional form. At the same time, an analysis of figure 11 would show that the high rate of dissipation, indicated by the presence of relatively small eddies, takes place in a region that is not coincident with the zone of maximum shear. In studies presently under way at the Iowa Institute, however, an anisotropic flow field is assumed and the dissipation term—in its more general form—is determined through use of a technique similar to that introduced by Laufer (1954). The results seem to indicate, for the first six diameters downstream from the nozzle, a dissipation term somewhat larger than the one evaluated from isotropic-flow-field assumptions.

3.4. *Intermittency*

The probability of occurrence of turbulence at any point within the flow field, called the 'intermittency factor' γ, was measured directly by an intermittency analyser. Figure 12 shows the distribution of the intermittency factor throughout the region of flow establishment. The extreme limits of turbulent motion and

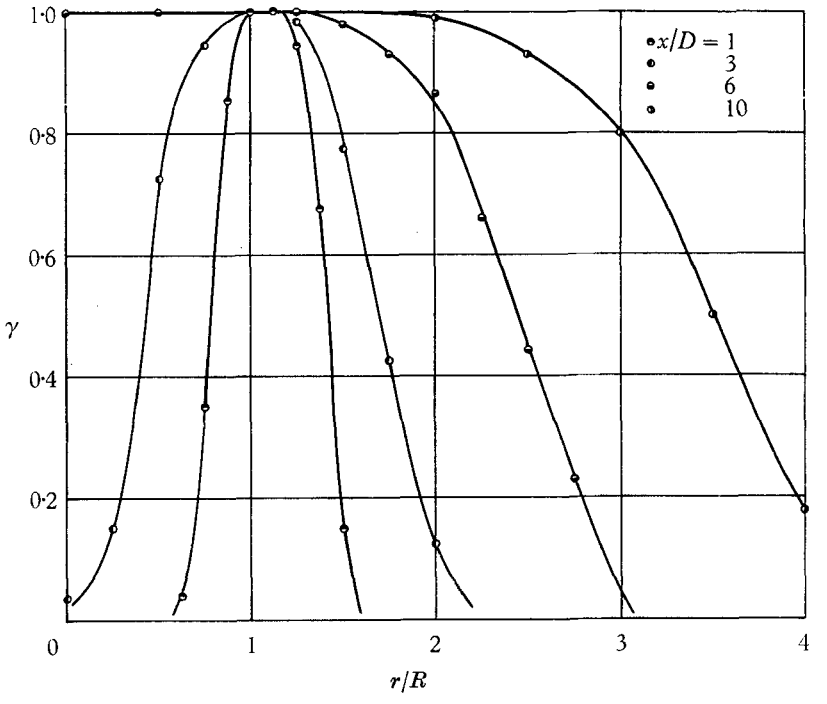

FIGURE 12. Intermittency factor.

mean-velocity variation, indicated by the distributions of intermittency factor and mean velocity, respectively, are in good agreement. However, obtaining the mean values of the axial turbulence intensity within the turbulent fluid alone represents a point of major interest. With an appropriate electronic circuitry combining the analyser output with the hot-wire-anemometer signal and through use of an electronic counter in the ratio mode, simultaneous readings of the two signals were reduced directly to the form $\overline{u'^2}/\gamma$. One serious restriction against this sort of treatment of the random variable was the necessity for it to be zero in the potential flow (Corrsin & Kistler 1955). Hence, the intermittency analyser was designed to eliminate all non-turbulent fluctuations of the random variable by shutting off the integration process each time the probe was within the potential part of the flow. The turbulence characteristics of the flow are still far from being uniform over the region. Well inside the zone of established flow of a two-dimensional jet, Bradbury (1965) found no evidence of a tendency on the part of the turbulence characteristics to approach near uniformity.

3.5. *Axial-momentum equation*

All the terms of both the integral and differential forms of the axial-momentum equation for an axisymmetric jet flow were experimentally evaluated throughout the field of measurement. They have been previously formulated and interpreted by one of the authors (Rouse 1960) for the case of axisymmetric flow. For the

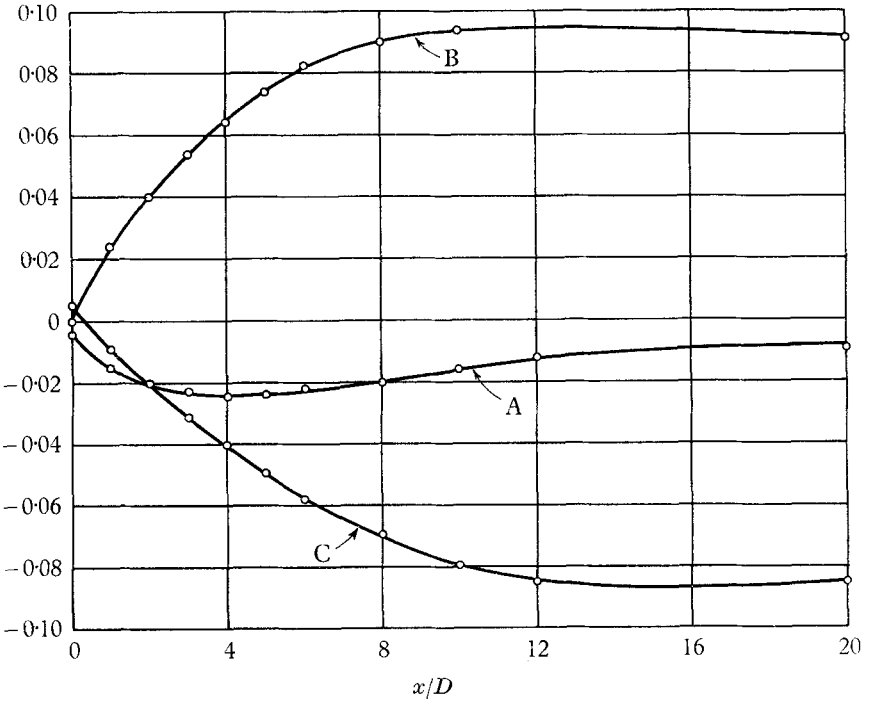

FIGURE 13. Momentum analysis—integral form (see equation (1)).

present case one has only to consider the fact that the relative upstream velocity is unity and the pressure has been referred to the efflux section. With that in mind, one can write the integral form of the axial momentum equation, for an axisymmetric jet, as follows:

$$\underbrace{2\int\left[\left(\frac{\overline{u}}{U}\right)^2-1\right]\frac{r}{R}d\frac{r}{R}}_{\text{A}}+\underbrace{2\int\frac{\overline{u'^2}}{U^2}\frac{r}{R}d\frac{r}{R}}_{\text{B}}+\underbrace{\int\frac{\overline{p}}{\frac{1}{2}\rho U^2}\frac{r}{R}d\frac{r}{R}}_{\text{C}}=0. \tag{1}$$

In its differential form, the equation becomes

$$\underbrace{\frac{1}{(r/R)}\frac{\partial}{\partial(x/R)}\left[\frac{r}{R}\left(\frac{\overline{u}}{U}\right)^2\right]}_{\text{I}}+\underbrace{\frac{1}{(r/R)}\frac{\partial}{\partial(r/R)}\left[\frac{r}{R}\frac{\overline{u}}{U}\frac{\overline{v}}{U}\right]}_{\text{II}}+\underbrace{\frac{1}{(r/R)}\frac{\partial}{\partial(x/R)}\left[\frac{r}{R}\left(\frac{\overline{u'^2}}{U^2}\right)\right]}_{\text{III}}$$

$$+\underbrace{\frac{1}{(r/R)}\frac{\partial}{\partial(x/R)}\left[\frac{r}{R}\left(\frac{\overline{p}}{\rho U^2}\right)\right]}_{\text{IV}}+\underbrace{\frac{1}{(r/R)}\frac{\partial}{\partial(r/R)}\left[\frac{r}{R}\left(\frac{\overline{u'v'}}{U^2}\right)\right]}_{\text{V}}=0. \tag{2}$$

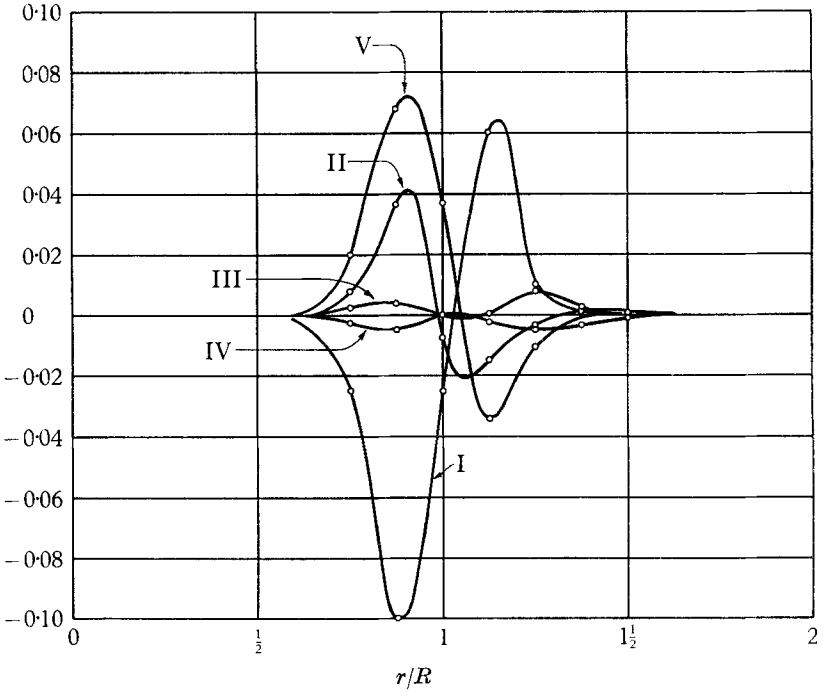

FIGURE 14. Momentum analysis at $x/D = 1$ (see equation (2)).

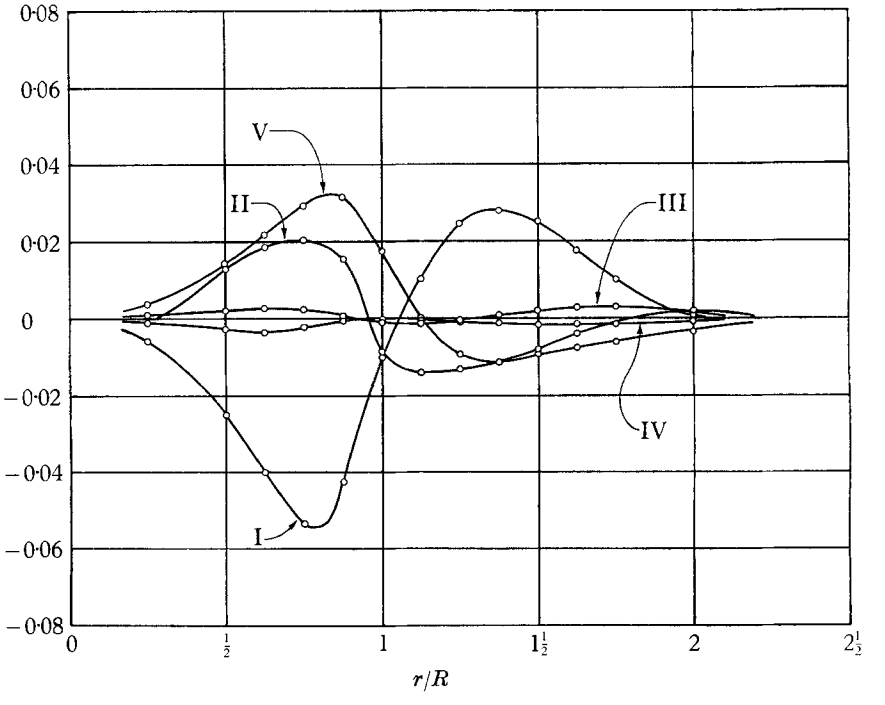

FIGURE 15. Momentum analysis at $x/D = 3$ (see equation (2)).

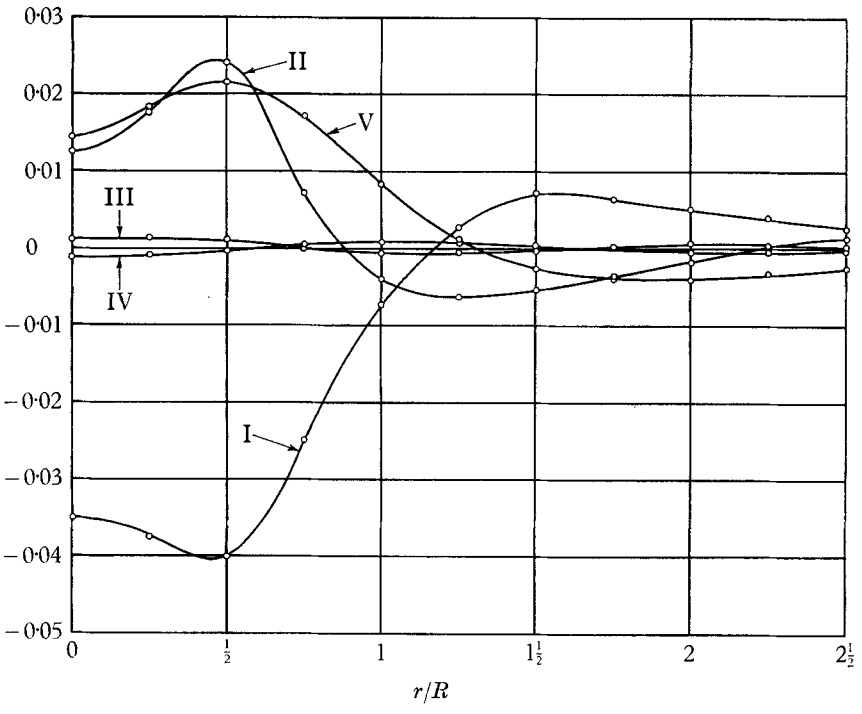

FIGURE 16. Momentum analysis at $x/D = 6$ (see equation (2)).

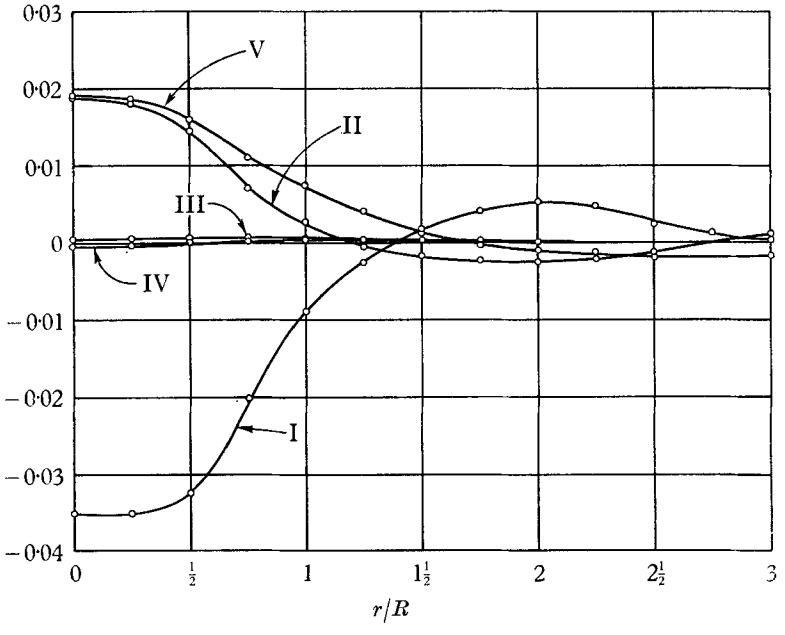

FIGURE 17. Momentum analysis at $x/D = 10$ (see equation (2)).

All the flow characteristics involved in the equation have already been presented in detail. The gradients of different variables were obtained from smoothed curves such as those presented in figures 3–8. The evaluated results are plotted for the integral form of the equation in figure 13 and for the differential form in figures 14–17. In both cases they do not deviate from the requirements of the relationship by more than 3 % of the differential momentum flux, thus providing a reasonable check of the measured data. In an effort to extend the analysis to the region of fully established flow, a similarity form of the momentum equation has been formulated by simply considering the similarity of velocity profiles at successive sections and the constancy of the momentum flux through the introduction of the relationship $(\overline{u}_m/U)(x/D) = C$. The various terms of the momentum equation for the region of established flow are plotted in figure 18.

3.6. *Mean-energy equation*

In order to complete the investigation, attention was ultimately given to a general energy analysis of the motion. Since both mean- and turbulence-energy considerations, for the particular case of an axisymmetric flow, have been formulated and discussed in the previously mentioned paper (Rouse 1960), they do not warrant any further interpretation at this time. The integral and differential mean-energy equations assume the following two non-dimensional forms, respectively:

$$\underbrace{2\int\left[\frac{\overline{u}}{\overline{U}}\left(\frac{\overline{V}}{\overline{U}}\right)^2-1\right]\frac{r}{R}d\frac{r}{R}}_{\text{a}}+\underbrace{2\int\frac{\overline{u}}{\overline{U}}\frac{\overline{p}}{\frac{1}{2}\rho\overline{U}^2}\frac{r}{R}d\frac{r}{R}}_{\text{b}}+\underbrace{4\int\left(\frac{\overline{u}}{\overline{U}}\frac{\overline{u'^2}}{\overline{U}^2}+\frac{\overline{v}}{\overline{U}}\frac{\overline{u'v'}}{\overline{U}^2}\right)\frac{r}{R}d\frac{r}{R}}_{\text{c}}$$

$$\underbrace{-4\int\int\left\{\frac{\overline{u'v'}}{\overline{U}^2}\left[\frac{\partial}{\partial(r/R)}\left(\frac{\overline{u}}{\overline{U}}\right)+\frac{\partial}{\partial(x/R)}\left(\frac{\overline{v}}{\overline{U}}\right)\right]+\frac{1}{2}\frac{\overline{u'^2}}{\overline{U}^2}\frac{\partial}{\partial(x/R)}\left(\frac{\overline{u}}{\overline{U}}\right)\right\}\frac{r}{R}d\frac{r}{R}d\frac{x}{R}}_{\text{d}}=0, \quad (3)$$

$$\underbrace{\left[\frac{\overline{u}}{\overline{U}}\frac{\partial}{\partial(x/R)}\left(\frac{\overline{p}}{\rho\overline{U}^2}\right)+\frac{\overline{v}}{\overline{U}}\frac{\partial}{\partial(r/R)}\left(\frac{\overline{p}}{\rho\overline{U}^2}\right)\right]}_{\text{i}}$$

$$+\underbrace{\frac{1}{(r/R)}\left[\frac{\partial}{\partial(x/R)}\frac{r}{R}\left(\frac{\overline{u}}{\overline{U}}\frac{\overline{u'^2}}{\overline{U}^2}+\frac{\overline{v}}{\overline{U}}\frac{\overline{u'v'}}{\overline{U}^2}\right)+\frac{\partial}{\partial(r/R)}\frac{r}{R}\left(\frac{\overline{u}}{\overline{U}}\frac{\overline{u'v'}}{\overline{U}^2}+\frac{\overline{v}}{\overline{U}}\frac{\overline{v'^2}}{\overline{U}^2}\right)\right]}_{\text{ii}}$$

$$+\underbrace{\frac{1}{2}\left[\frac{\overline{u}}{\overline{U}}\frac{\partial}{\partial(x/R)}\left(\frac{\overline{V}}{\overline{U}}\right)^2+\frac{\overline{v}}{\overline{U}}\frac{\partial}{\partial(r/R)}\left(\frac{\overline{V}}{\overline{U}}\right)^2\right]}_{\text{iii}}$$

$$-\underbrace{\left\{\frac{\overline{u'v'}}{\overline{U}^2}\left[\frac{\partial}{\partial(r/R)}\left(\frac{\overline{u}}{\overline{U}}\right)+\frac{\partial}{\partial(x/R)}\left(\frac{\overline{v}}{\overline{U}}\right)+\frac{1}{2}\frac{\overline{u'^2}}{\overline{U}^2}\frac{\partial}{\partial(x/R)}\left(\frac{\overline{u}}{\overline{U}}\right)\right\}}_{\text{iv}}=0. \quad (4)$$

The turbulence-energy counterparts of these equations will not be considered in this paper. The Iowa Institute is at present carrying out a complete turbulence-energy analysis, in the course of which all pertinent terms of the equation are to

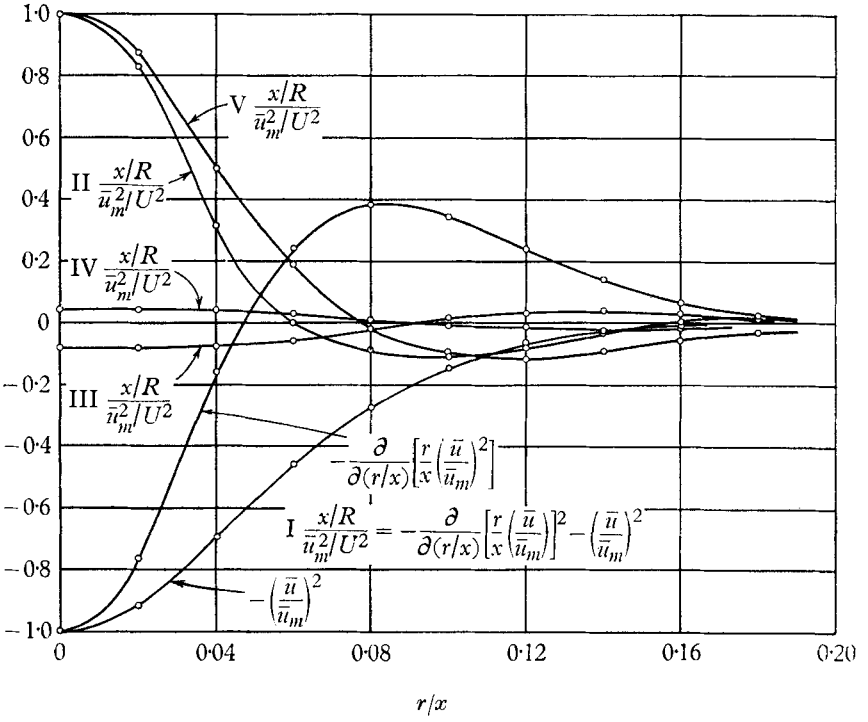

FIGURE 18. Momentum analysis for the zone of established flow.

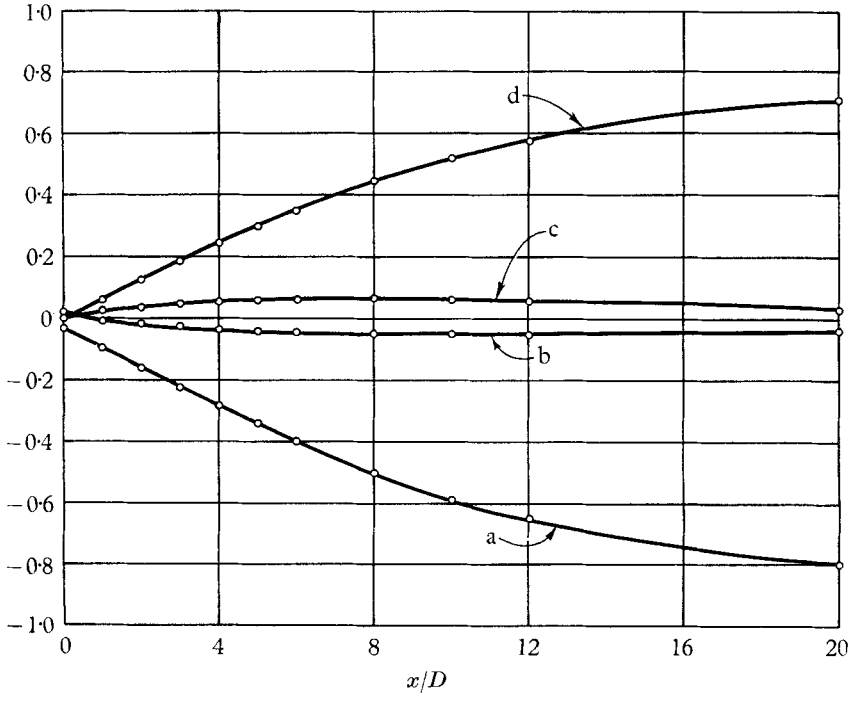

FIGURE 19. Mean-energy analysis—integral form (see equation (3)).

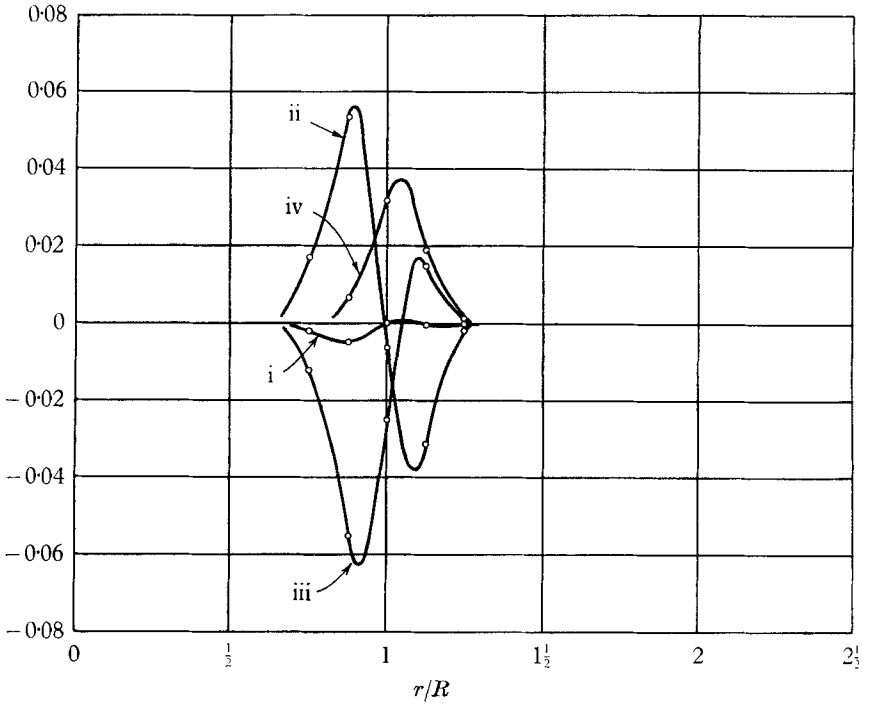

FIGURE 20. Mean-energy analysis at $x/D = 1$ (see equation (4)).

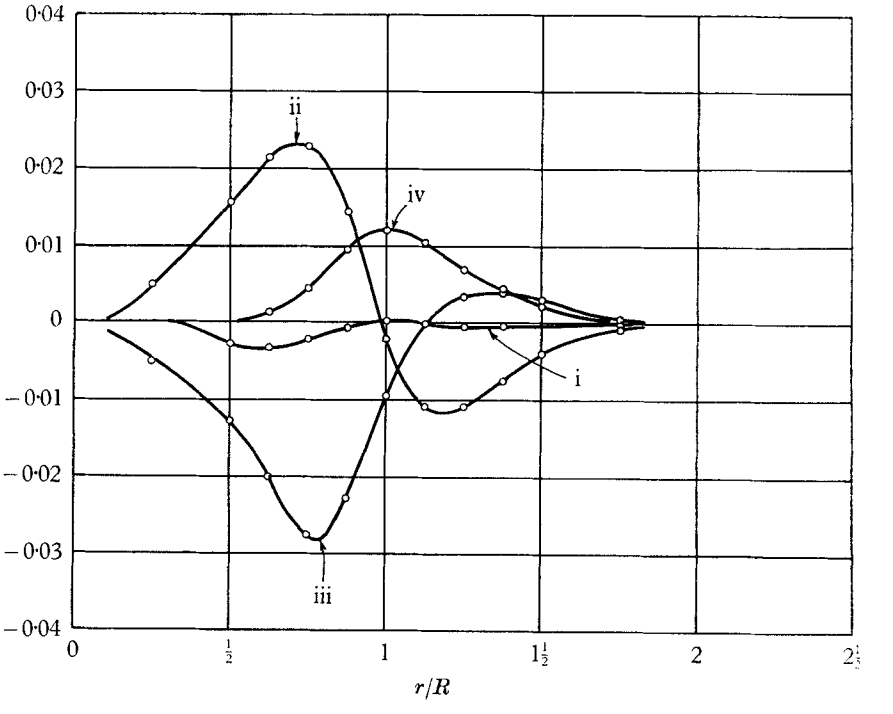

FIGURE 21. Mean-energy analysis at $x/D = 3$ (see equation (4)).

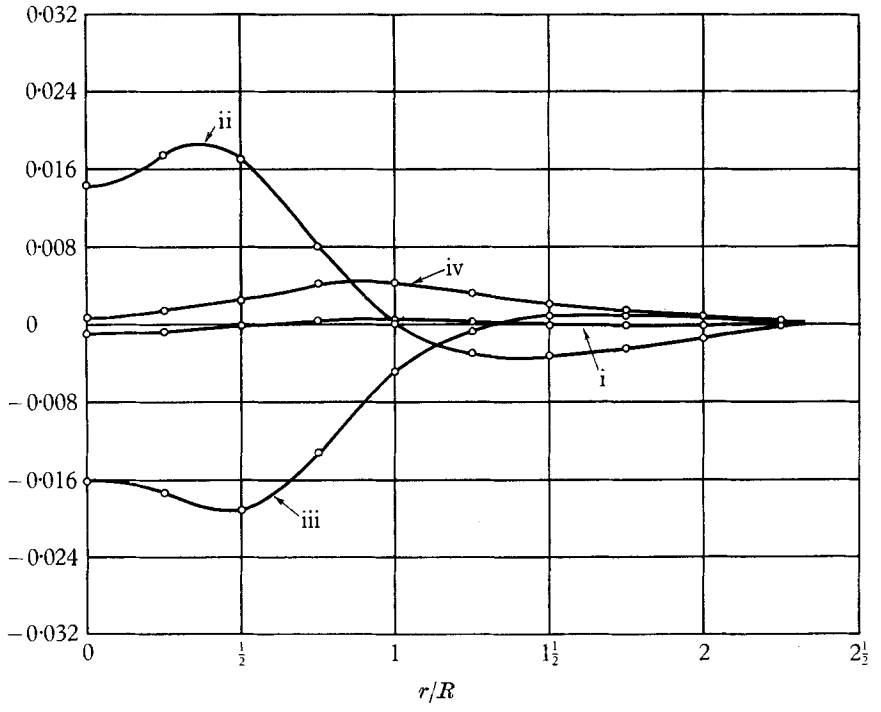

FIGURE 22. Mean-energy analysis at $x/D = 6$ (see equation (4)).

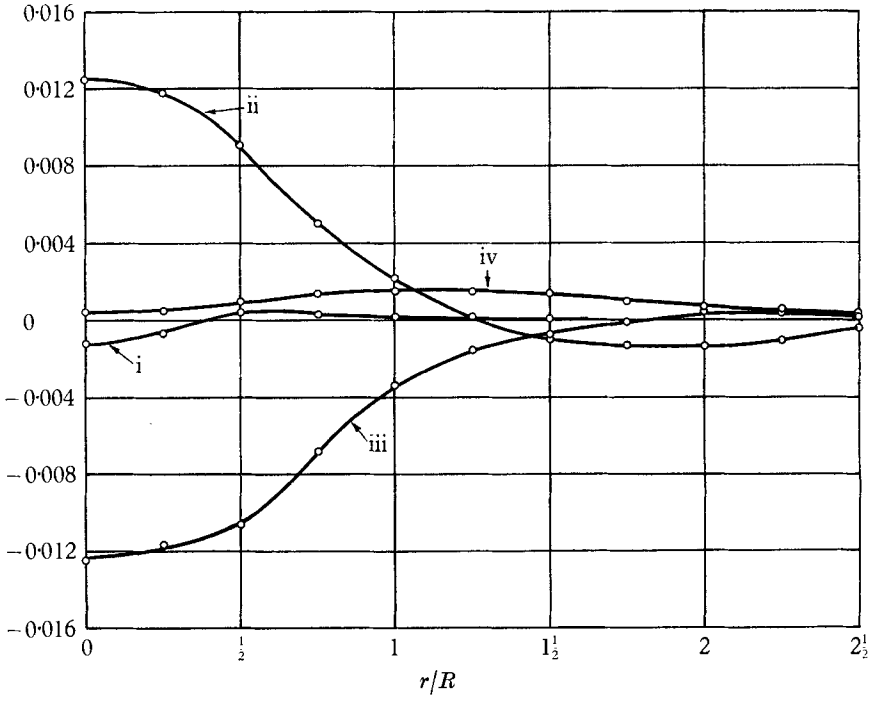

FIGURE 23. Mean-energy analysis at $x/D = 10$ (see equation (4)).

be evaluated from properly measured characteristics of turbulence at all points. Results for the mean-energy equation, obtained by evaluating each term section by section or pointwise, are given for the integral form of the equation in figure 19 and for the differential form in figures 20–23. The balancing of the two equations is performed by summing ordinates of the various terms at a given cross-section (integral form) or at a given point (differential form). They meet the requirements of the relationship within 5 % of the differential energy flux. For the region of established flow, the terms of the mean-energy equation—in its similarity form—are plotted in figure 24.

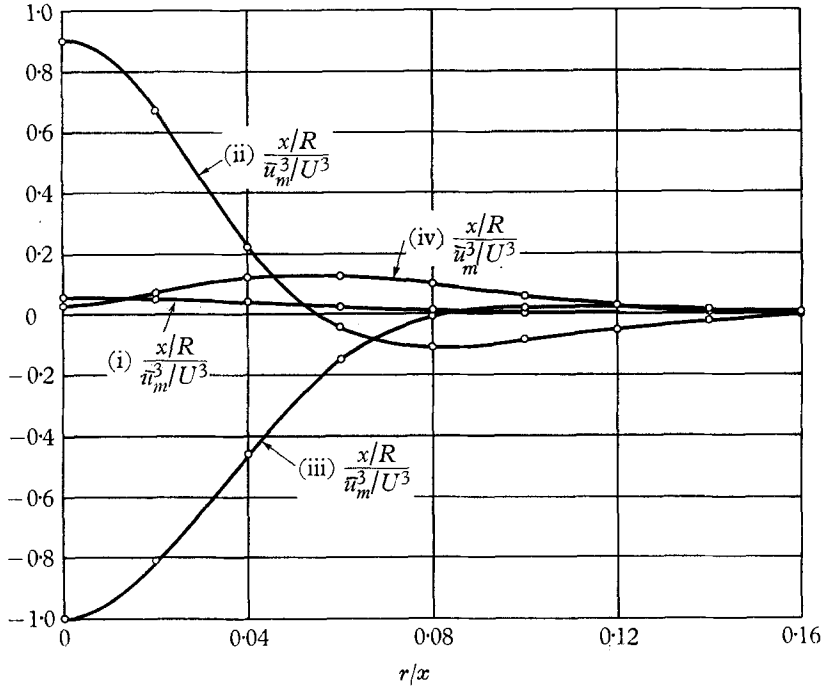

FIGURE 24. Mean-energy analysis for the zone of established flow.

4. Conclusion

In the course of a general investigation of the fundamental mean-flow and turbulence characteristics of a diffusing jet, the fluctuating pressure was given particular attention, and a probe of the piezo-electric type was developed and used to measure the pressure fluctuations throughout the field of motion. In the region of flow establishment, the distribution of the fluctuation was found to be similar to that of the turbulence intensity. As part of an investigation of the eddy concept of turbulence, both the large scale and the micro-scale were measured. The former was seen to be independent of the jet velocity; in the region of flow establishment, it was also seen to increase with distance from the efflux section. Dissipation-length measurements, on the other hand, appear to support earlier observations as to the structure of the small-scale eddies: those with a relatively low frequency are located near the axis of the jet, while the higher-frequency

eddies seem to appear in the vicinity of the nominal boundary of the jet. The results of intermittency measurements have shown that, in the region of flow establishment, the mean axial-turbulence intensities within the jet are not uniform. A detailed evaluation of all the terms of the momentum and mean-energy equations for the region of flow establishment, in both integral and differential forms, indicates that a satisfactory representation of the mean flow is now at hand. A significant illustration is also provided of the relations prevailing among the various factors involved in the dynamics of the motion in general and in the production of turbulence in particular.

For the past two decades the programme of jet-diffusion studies at Iowa has proceeded under the direction of the third author. Research assistance has been rendered in recent years by K. C. Peng, S. R. Carr, and R. G. Hajek, and valuable aid in instrumentation by Drs P. G. Hubbard and J. R. Glover, staff members of the Iowa Institute of Hydraulic Research. The experimental results presented herein were obtained and analysed by the second author and the first, successively Research Associates of the Iowa Institute. The paper itself was written and illustrated by the first author. All phases of the programme were supported by the Office of Naval Research under Contract Nonr 1509(03) with the Institute.

REFERENCES

ALEXANDER, L. G., BARON, T. & COMINGS, E. W. 1953 Transport of momentum, mass and heat in turbulent jets. *Univ. of Illinois Engng. Exp. Sta. Bulletin*, no. 413.

BAINES, W. D. 1948 Investigations in the diffusion of submerged jets. M.S. thesis, University of Iowa.

BRADBURY, L. J. S. 1965 The structure of a self-preserving turbulent plane jet. *J. Fluid Mech.* **23**, 31.

CARMODY, T. 1964 Establishment of the wake behind a disk. *Trans. ASME J. Basic Engng.* **86**, 869.

CHATURVEDI, M. D. 1963 Flow characteristics at abrupt axisymmetric expansions. *Proc. ASCE J. Hydr. Div.* **89**, 61.

CORRSIN, S. 1947 Investigation of the flow in an axially symmetric heated jet. *NACA Rept.* no. W-94.

CORRSIN, S. & KISTLER, A. L. 1955 Free-stream boundaries of turbulent flows. *NACA Rept.* no. 1244.

CORRSIN, S. & UBEROI, M. S. 1949 Further experiments on the flow and heat transfer in a heated turbulent air jet. *NACA TN* no. 1865.

DAI, Y. B. 1947 Distribution of velocity in turbulent jets of air. M.S. Thesis, University of Iowa.

DAVIES, P. A. O. L., FISHER, M. J. & BARRATT, M. J. 1963 The characteristics of the turbulence in the mixing region of a round jet. *J. Fluid Mech.* **15**, 337.

GLOVER, J. R. 1965 Techniques for detecting and analysing unsteady flow variables. Ph.D. dissertation, University of Iowa.

HINZE, J. O. & VAN DER HEGGE ZIJNEN, B. G. 1949 Transfer of heat and matter in the turbulent mixing zone of an axially symmetrical jet. *Appl. Sci. Res.* A-**1**, 435.

KOBASHI, Y. 1957 Measurements of pressure fluctuation in the wake of a cylinder. *J. Phys. Soc. Japan* **12**, 533.

LAUFER, J. 1954 The structure of turbulence in a fully developed pipe flow. *NACA Rep.* no. 1174.

LAURENCE, J. C. 1956 Intensity, scale, and spectra of turbulence in the mixing region of a subsonic jet. *NACA Rep.* no. 1292.

MILLER, D. R. & COMINGS, E. W. 1957 Static pressure distribution in the free turbulent jet. *J. Fluid Mech.* **3**, 1.

NAUDASCHER, E. 1965 Flow in the wake of self-propelled bodies and related sources of turbulence. *J. Fluid Mech.* **22**, 625.

ROUSE, H., SIAO, T. T. & NAGARATNAM, S. 1959 Turbulence characteristics of the hydraulic jump. *Trans. ASCE* **124**, 926.

ROUSE, H. 1953 Cavitation in the mixing zone of a submerged jet. *La Houille Blanche*, nos. 1 and 2.

ROUSE, H. 1960 Distribution of energy in regions of separation. *La Houille Blanche*, nos. 3 and 4.

STRASBERG, M. 1963 Measurements of the fluctuating static and total-head pressures in a turbulent wake. *David Taylor Model Basin Rept.* no. 1779.